Acta Crystallographica Section D
Biological Crystallography
ISSN 0907-4449

Exploration of the GM1 receptor-binding site of heat-labile enterotoxin and cholera toxin by phenyl-ring-containing galactose derivatives

Erkang Fan,[a] Ethan A. Merritt,[a] Zhongsheng Zhang,[a] Jason C. Pickens,[a,c] Claudia Roach,[b] Misol Ahn[a] and Wim G. J. Hol[a,b,d]*

[a]Department of Biological Structure, Box 357742, University of Washington, Seattle, WA 98195, USA, [b]Howard Hughes Medical Institute, Box 357742, University of Washington, Seattle, WA 98195, USA, [c]Department of Chemistry, Box 351700, University of Washington, Seattle, WA 98195, USA, and [d]Department of Biochemistry, Box 357742, University of Washington, Seattle, WA 98195, USA

Correspondence e-mail: hol@gouda.bmsc.washington.edu

Received 25 July 2000
Accepted 9 November 2000

PDB References: LT*B*–PAPG, 1efi; CT*B*–MNPG, 1eei; LT*B*–BAPG, 1fd7; LT*B*–PEPG, 1eef.

Cholera toxin (CT) and the closely related heat-labile enterotoxin of *Escherichia coli* (LT) are responsible for numerous cases of diarrhea worldwide, leading to considerable morbidity and mortality. The *B* subunits of these heterohexameric AB_5 toxins form a pentameric arrangement which is responsible for binding to the receptor GM1 of the target epithelial cells of the host. Blocking these *B* pentamer–receptor interactions forms an avenue for therapeutic intervention. Here, the structural characterization of potential receptor-blocking compounds are described based on the previously identified inhibitor *m*-nitrophenyl-α-D-galactoside (MNPG). The structure of a CT*B*–MNPG complex confirms that the binding mode of this inhibitor is identical in the two homologous toxins CT and LT and is characterized by a glycosyl linkage geometry that leads to displacement of a well ordered water molecule near the amide group of Gly33 by the O1-substituent of MNPG. This glycosyl geometry is not maintained in the absence of a substituent that can displace this water, as shown by a complex of LT*B* with *p*-aminophenyl-α-D-galactoside (PAPG). New compounds were synthesized to investigate the feasibility of maintaining the favorable binding interactions exhibited by MNPG while gaining increased affinity through the addition of hydrophobic substituents complementary to either of two hydrophobic regions of the receptor-binding site. The structural characterization of complexes of LT*B* with two of these compounds, 3-benzyl-aminocarbonylphenyl-α-D-galactoside (BAPG) and 2-phenethyl-7-(2,3-dihydrophthalazine-1,4-dione)-α-D-galactoside (PEPG), demonstrates a partial success in this goal. Both compounds exhibit a mixture of binding modes, some of which are presumably influenced by the local packing environment at multiple crystallographically independent binding sites. The terminal phenyl ring of BAPG associates either with the phenyl group of Tyr12 or with the hydrophobic patch formed by Lys34 and Ile58. The latter interaction is also made by the terminal phenyl substituent of PEPG, despite a larger ring system linking the galactose moiety to the terminal phenyl. However, neither BAPG nor PEPG displaces the intended target water molecule. Both of the designed compounds exhibit increased affinity relative to the galactose and to PAPG notwithstanding the failure to displace a bound water, confirming that additional favorable hydrophobic interactions can be gained by extending the starting inhibitor by a hydrophobic tail. The insight gained from these structures should allow the design of additional candidate inhibitors that retain both the glycosyl geometry and water displacement exhibited by MNPG and the favorable hydrophobic interactions exhibited by BAPG and PEPG.

1. Introduction

Heat-labile enterotoxin (LT) and cholera toxin (CT) are two closely related AB_5 heterohexameric molecules secreted by enterotoxigenic *E. coli* and *Vibrio cholerae*, respectively. LT causes traveler's diarrhea and is also responsible for the death by dehydration of hundreds of thousands of children each year in developing countries (Wanke *et al.*, 1987; Holmgren & Svennerholm, 1992). CT is the causative agent of cholera, which has 370 000 cases worldwide each year with a lethality rate of more than 3% (Simeant, 1992). There is currently no prophylaxis against LT or CT and there are only short-lasting vaccines against *V. cholerae*. Therapeutic treatment for either LT- or CT-caused diarrhea is very labor intensive. Therefore, the development of novel drugs for the treatment and/or prevention of LT- and CT-caused diseases is of great importance.

Both toxins are heterohexamers which are assembled in the periplasm of the bacterium and consist of one *A* subunit and five identical *B* subunits. The *A* and *B* subunits have entirely different but essential functions. The toxin's *A* subunit is responsible for ADP-ribosylation of the regulatory protein $G_{s\alpha}$ in host epithelial cells, while the *B* pentamer binds with high affinity to saccharides on the surface of the epithelial cells of the gastrointestinal tract. The receptor for CT and the major receptor for LT is the pentasaccharide of ganglioside GM1 [Gal(β1–3)GalNAc(β1–4){NeuAc(α2–3)}Gal(β1–4)Glc(β1–1) ceramide] (Eidels *et al.*, 1983; Schengrund & Ringler, 1989). Since the binding of the toxin's *B* pentamer to its cellular surface receptor is a critical step in translocating the toxin into epithelial cells, blocking the receptor-binding site of LT and CT with high-affinity ligands is an attractive way to prevent LT and CT from entering the host target cell. Such ligands are leads for the development of novel compounds to treat and prevent diseases caused by *V. cholerae* and enterotoxigenic *E. coli*.

Previously determined crystal structures of heat-labile enterotoxin revealed for the first time the remarkable architecture of an AB_5 toxin, with the *A* subunit located on the opposite side of the *B* pentamer from the GM1 receptor-binding sites (Sixma *et al.*, 1991, 1992, 1993). The binding mode of five copies of the GM1 pentasaccharide to the *B* pentamer of CT has been very well characterized by a crystal structure determination at 1.25 Å resolution (Merritt *et al.*, 1998). The interaction of LT with a number of saccharides and galactose derivatives has been studied crystallographically (Sixma *et al.*, 1992; van den Akker *et al.*, 1996; Merritt *et al.*, 1997; Minke *et al.*, 2000) and has also been the subject of computational studies (Minke, Diller *et al.*, 1999; Minke, Roach *et al.*, 1999) and combinatorial chemistry approaches (Minke, Hong *et al.*, 1999). These studies revealed the position of a number of well defined 'canonical' water molecules (sites #1–#10; Merritt, Sixma *et al.*, 1994).

Galactose itself (β-D-galactopyranose) binds to the toxins with relatively low affinity (with IC_{50} values in the ELISA assay of 58 m*M* for LT and 45 m*M* for CT; Minke, Roach *et al.*, 1999), with an essentially identical binding mode as the terminal galactose of the GM1 pentasaccharide (Merritt, Sixma *et al.*, 1994). Galactose alone occupies only a fraction of the full receptor-binding site, yet makes numerous interactions with the *B* subunit and hence retains its binding mode despite a wide variety of substitutions at the C1 position. Therefore, the galactose moiety can serve as an 'anchor' to explore favorable interactions of O1-substituents with other portions of the binding site. One such derivative, *m*-nitrophenyl-α-D-galactoside (MNPG) was discovered from an initial screen of commercially available galactose variants and derivatives (Minke, Roach *et al.*, 1999). Two key features of the MNPG binding mode were identified from the structure of an LT*B*–MNPG complex (Merritt *et al.*, 1997). The presence of an α-linkage rather than the β-linkage found in the natural receptor is not only tolerated by the binding site but allows an α-linked O1 substituent to conform more closely to the surface of the binding site, resulting in better shape complementarity. Furthermore, the nitrophenyl substituent adopts a conformation that places one of the nitro O atoms exactly on top of the canonical water-binding site #2, where it duplicates the hydrogen-bonding network otherwise formed by the displaced water molecule. MNPG occupies less than half of the receptor-binding pocket, leaving substantial scope for improving its binding affinity through the addition of further chemical substituents. In particular, we have identified two hydrophobic patches on the receptor-binding surface which remain exposed after MNPG binding. One of these is formed by the face of the phenyl group in the side chain of Tyr12; the other is formed by the backbone and side chains of residues Lys34 and Ile58. In designing larger candidate inhibitors, we have attempted to retain the chemical scaffold and key features of the MNPG binding mode while linking this scaffold to a hydrophobic group that can associate with one or both of these hydrophobic patches.

We report here four structures relevant to this line of improved inhibitor design (structures and IC_{50} values shown in Fig. 1). The complex of MNPG with CT*B* confirms that the binding mode of this scaffold is identical in the two homologous toxins CT and LT. This is in fact the first ligand for which structures complexed both with LT and with CT are available. The complex of *p*-aminophenyl-α-D-galactoside (PAPG) with LT*B* indicates that one key feature of the MNPG binding mode, the conformation of the glycosyl linkage, is not retained in the absence of the *meta* substituent. The two remaining structures are of LT*B* complexed with larger inhibitors, BAPG and PEPG, which were synthesized specifically to explore the addition of hydrophobic substituents to the MNPG scaffold (Fig. 1).

These structures confirmed the invariant binding mode of galactose but revealed that phenyl derivatives attached at the galactose O1 position adopted a variety of conformations about the linking bonds, even when they share a common substructure. In particular, the specific favorable interactions observed for the bound conformation of MNPG were not retained by isosteric moieties of the larger ligands BAPG and PEPG. The multiplicity of the observed binding sites, ranging from five to ten copies per structure solved, provides a wealth

Table 1
Crystallographic data.

	CT*B*–MNPG	LT*B*–PAPG	LT*B*–BAPG	LT*B*–PEPG
PDB code	1eei	1efi	1fd7	1eef
Space group	$P2_12_12_1$	$P2_1$	$P2_1$	$P2_1$
Unit-cell parameters				
a (Å)	68.90	42.65	60.76	88.54
b (Å)	69.55	96.34	157.54	65.02
c (Å)	130.66	63.58	63.15	101.93
β (°)		107.3	116.5	115.5
Pentamers per asymmetric unit	1	1	2	2
V_M (Å^3 Da^{-1})	2.6	2.1	2.5	2.2
Data collection				
Unique data measured	40887	50240	79747	97336
Completeness (highest shell) (%)	93 (88)	78 (54)	81 (76)	94 (99)
R_{merge} on intensities	0.064 (0.276)	0.035 (0.055)	0.050 (0.132)	0.051 (0.115)
Data used in refinement				
Reflections (working set)	38380	48196	75687	92116
Reflections (R_{free} set)	1982	2034	3960	4889
Cutoffs (Å)	20–2.0, $F/\sigma(F) > 1.0$	25–1.6, $F/\sigma(F) > 1.0$	20–1.8	22–1.8, $F/\sigma(F) > 1.0$
Model				
R	0.200	0.188	0.187	0.182
R_{free}	0.251	0.231	0.234	0.267
Protein atoms (B_{avg}, Å^2)	4070 (25)	4120 (12)	8240 (17)	8240 (16)
Ligand atoms (B_{avg}, Å^2)	105 (30)	95 (15)	297 (26)	200 (15)
Water molecules (B_{avg}, Å^2)	455 (45)	695 (34)	856 (21)	1085 (30)
Stereochemistry				
R.m.s. non-ideality, bond lengths (Å)	0.011	0.010	0.012	0.013
R.m.s. non-ideality, bond angles (°)	1.58	1.54	1.80	1.58
R.m.s. ΔB between bonded atoms (Å^2)	3.1	2.1	1.4	2.3

of information to evaluate the variability in ligand-binding modes, the flexibility of the protein and the rearrangement of water molecules in the various complexes studied. The observed substituent-binding modes provide a basis for further improvement of the affinity of galactose derivatives targeting the receptor-binding site of LT and CT.

2. Results

The crystal structures reported in this paper (Table 1) resulted in 30 views of the LT/CT *B*-subunit with a substituted phenyl-α-galactoside molecule bound to the receptor-binding site of each subunit. In all 30 examples, the galactose moiety is well defined and binds in the canonical mode to LT and CT (Sixma *et al.*, 1992; Merritt, Sartafy *et al.*, 1994; Merritt, Sixma *et al.*, 1994). In contrast, the bound conformations of the phenyl-containing O1 substituents vary widely.

In the case of MNPG in complex with CT*B* solved at a resolution of 2.0 Å, all five binding sites are well occupied and not only the galactoside units but also the five crystallographically independent *m*-nitrophenyl moieties are well defined and adopt essentially the same position. Also, all but one of the 'canonical' waters (Merritt *et al.*, 1997) are well defined in each binding site. When all five sites are mutually superimposed, the r.m.s. deviation from the mean position for the 12 galactose C and O atoms is 0.37 Å, while for the *m*-nitrophenyl groups the r.m.s. deviation is 0.43 Å. In all five instances, the O2′ of the nitrophenyl group has displaced water #2 – exactly as in the LT*B*–MNPG complex (Fig. 2). The other water sites mediating toxin–galactose hydrogen bonding are in excellent agreement in the LT and CT complexes. After superposition of all 15 copies of the toxin *B* subunit, 11 observed waters at site #1 cluster to within 0.65 Å, 15 observed waters at site #3 cluster to within 0.65 Å and 13 observed waters at site #5 fall within 0.8 Å of each other. Clearly, all aspects of MNPG binding by CT are not only essentially identical in each of the five CT*B* subunits, but also very similar to those observed in the LT*B*–MNPG complex (Fig. 2).

In the case of PAPG, the situation is different with respect to the number of binding modes of the O1 substituent, as revealed in the crystal structure of the LT*B*–PAPG complex solved at 1.6 Å resolution. While the five galactose moieties superimpose with an r.m.s. deviation of 0.36 Å, the *p*-aminophenyl units surprisingly occupy a range of positions with an r.m.s. deviation of 1.96 Å; the largest difference in position of the amino nitrogen is 2.5 Å (Fig. 3). In addition, the *p*-aminophenyl group of PAPG adopts a significantly different conformation to the *m*-nitrophenyl moiety of MNPG (Fig. 3) owing to the change of substitution pattern on the phenyl ring and as a consequence, no water molecules in the binding site are displaced upon PAPG binding. In spite of the variation in O1 substituent positions observed in the LT*B*–PAPG complex, the five canonical waters are in essentially the same position in each of the five binding sites. The *p*-aminophenyl group appears in most cases to be contacting the side chain of Tyr12, which is slightly shifted relative to its observed conformation in other toxin–ligand structures. The amino group does not interact with the protein either directly or through water-mediated hydrogen bonding.

The LT*B*–BAPG complex contains ten crystallographically independent binding sites and the ligand-binding mode is evident for all of these. Seven of the ten sites exhibit a single ligand-binding mode in which the terminal phenyl ring stacks against Tyr12. Two of the remaining binding sites are closely associated with each other owing to lattice packing and in these sites a different binding mode is seen in which the terminal phenyl ring is rotated about the N1′—C1* bond in such a way that the two lattice-related phenyl rings can stack with each other rather than with the side chain of Tyr12. In the tenth binding site, two binding modes are observed; one is identical to that seen in the two lattice-related binding sites, while the other places the terminal phenyl ring against the side chain of Lys34. These three binding modes (Fig. 4) will be

referred to as 'primary', 'secondary' and 'tertiary' because of their relative frequency of occurrence in the structure. In the primary and secondary binding modes, ligand atom O1′ lies 1.5 Å from the canonical water site #10. The ligand does not, however, duplicate the specific hydrogen-bonding interactions previously found for the water at this site. Well ordered electron density, indicating tightly associated water molecules, is present at canonical water sites #1, #2, #3, #4, #5, #7 and #9 (Fig. 4), with each site occupied in most or all of the ten crystallographically independent copies. In both the primary and secondary ligand conformations there is one water-mediated hydrogen-bonding link from ligand atom N1′ to the backbone carbonyl of Gly33 and another water-mediated hydrogen-bonding link from ligand atom O1′ to the backbone carbonyl of Arg13.

The conjugated ring system of PEPG (Fig. 1) can in principle interact with the protein through either hydrophobic or polar interactions, while the phenethyl group offers additional possibilities for hydrophobic interactions. Since the asymmetric unit contains two LT*B*–PEPG complexes, ten copies of the binding site are available to analyze the binding mode of this ligand to LT (Fig. 5). In four of the ten copies of the binding site in the crystal structure, a lattice interaction allows the conjugated ring system to stack parallel to a symmetry-related copy of itself. This interaction stabilizes a single conformation of the bound ligand. At these sites, the electron density for the entire compound is beautifully clear (Fig. 5*a*) and establishes the regiochemistry of the synthesized compound to be that shown in Fig. 1. In this conformation, the terminal phenyl group makes favorable non-polar interactions with the side chains of Lys34 and Ile58. In these four instances, the conformation of the sugar to phthalhydrazide linkage is shifted relative to that of MNPG by a rotation of 30° about the O1—C7 bond. The canonical water Wat2 is not displaced by PEPG as it is by MNPG, but instead mediates hydrogen bonding between O13 of the ligand and the protein backbone at residue Gly33 (Figs. 5*a* and 5*c*). There is well defined electron density for water at site #2, as well as for the other canonical waters, in all ten instances of PEPG interacting with the receptor-binding site.

In the six copies of the binding site at which the phthalhydrazide ring systems of PEPG are not involved in lattice-packing contacts, the electron density for this portion of the ligand is less well defined. Nevertheless, the galactose density remains clear, indicating that the ligand is indeed bound at these sites and the remaining density is at least consistent with the ligand-binding mode seen at the four lattice-stabilized sites. In some sites, the density is clear enough to suggest that this is the predominant binding mode, although not the only mode, even in the absence of stabilizing lattice interactions (Fig. 5*b*). This is quite plausible, as the favorable hydrophobic interactions between the terminal phenyl ring of the ligand

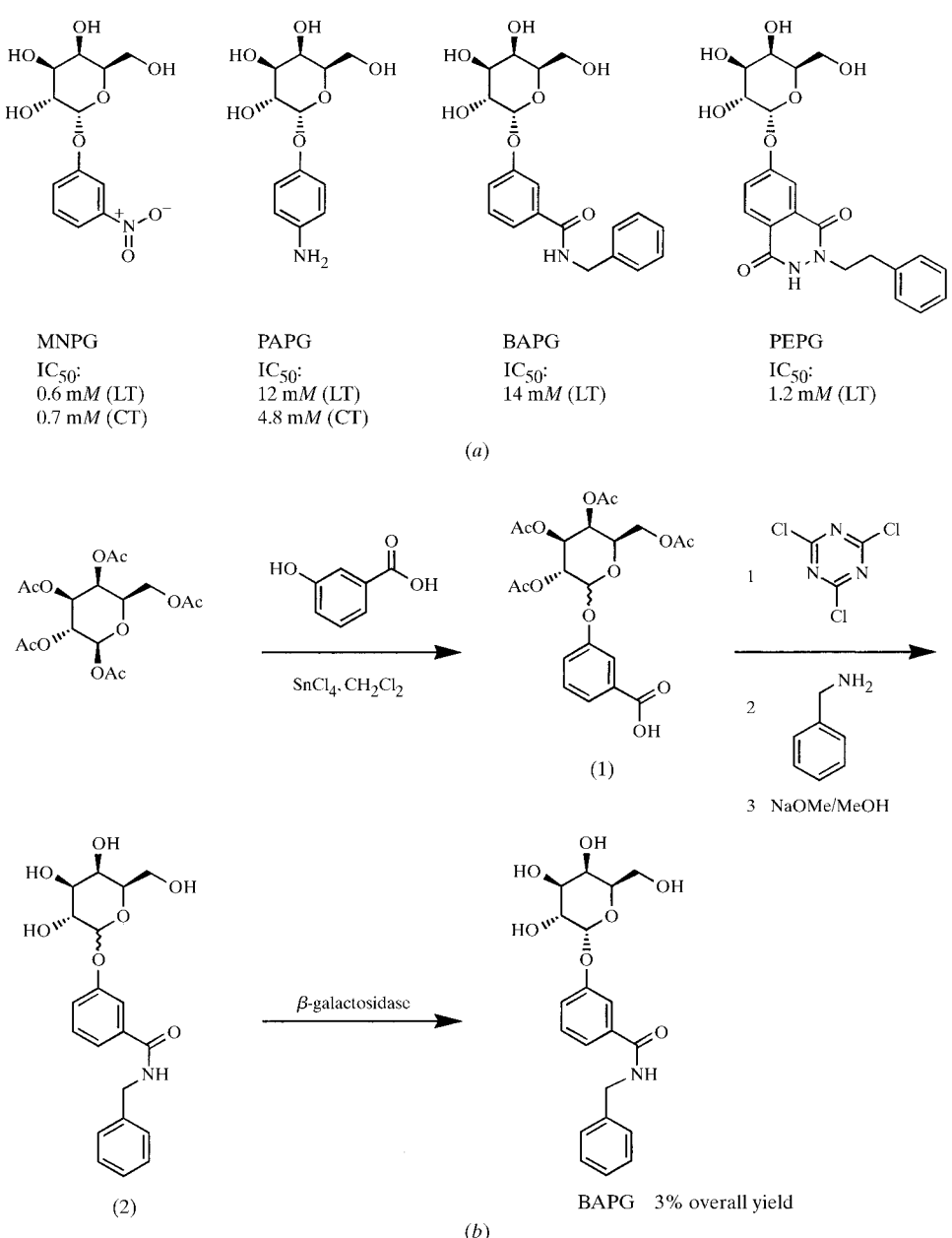

Figure 1
(*a*) Chemical structures and IC_{50} values of compounds investigated. (*b*) Synthesis scheme of 3-benzylaminocarbonylphenyl-α-D-galactoside (BAPG).

and protein residues Ile58 and Lys34 can probably accommodate some variation in the precise conformation of the phthalhydrazide ring system linking it to the anchoring galactose moiety. In the absence of conformational restriction owing to neighboring pentamer atoms, this variation is presumably sufficient to allow the terminal phenyl group to adopt a constellation of alternative positions along the binding site (upper portion of Fig. 5*b*) in addition to the predominant binding mode. When this conformational variation is restricted by lattice interactions, only the one predominant conformation is seen (Fig. 5*a*). This is quite encouraging from the perspective of further optimizing the binding of related compounds, as conformational restriction can also be introduced through further chemical modification of the ligand itself.

3. Discussion

Of the set of galactose derivatives initially characterized (Minke, Roach *et al.*, 1999), the lowest IC_{50} was found for *m*-nitrophenyl-α-galactoside (MNPG). The crystal structure of the LT*B*–MNPG complex (Merritt *et al.*, 1997) suggested aspects of the interaction mode contributing to the binding affinity worth exploring in subsequent ligand-design trials (Minke, Hong *et al.*, 1999; Minke, Roach *et al.*, 1999). The first aspect is the α-linkage of the substituent to the galactose, a geometry which places the O1 substituent closer to the surface of the protein than is seen for the β-linked GalNAc moiety of the natural GM1 pentasaccharide. The second feature, unique to MNPG, is the displacement of the highly conserved water at site #2 of the receptor binding surface by one O atom of the nitrophenyl group. The structures reported here explore the degree to which α-linked O1 substituents may be extended to fill the toxin's receptor-binding site, gaining affinity by adding hydrophobic groups which interact favorably with the protein.

The CT*B*–MNPG complex reported here represents the first time we have characterized equivalent complexes of a ligand with both LT*B* and CT*B*. The binding mode of the ligand to the two toxins is essentially the same, as is the conformation of the protein residues contributing to the receptor-binding site. When protein residues at the binding site in the LT*B*–MNPG and CT*B*–MNPG structures are superimposed (Fig. 2), the overall r.m.s. deviation in atomic coordinates is 0.32 Å for 157 protein atoms and 0.53 Å for the ligand atoms, indicating that the protein conformations as well as the ligand-binding modes are identical to within the accuracy of the structure determinations. The only sequence difference between the toxins in the immediate region of the binding site occurs at position 13, which is a His in CT and an Arg in LT. This residue may play a role in fine-tuning the specific recognition of the full receptor ganglioside GM1, but is not involved in binding MNPG. In both the LT*B*–MNPG and CT*B*–MNPG complexes, the water at site #2 is displaced by the nitro group. The hydrogen-bonding interactions normally associated with this water are maintained by the nitrophenyl O atom and cause the MNPG ligand to bind with virtually the same conformation to each toxin, now observed 15 times over between the crystal structures of LT and CT in complex with this ligand.

By contrast, the *p*-aminophenyl group of the ligand in the LT*B*–PAPG complex is not able to replace the water at site #2 and is not held in a single conformation. In the five copies of the binding site in the LT*B*–PAPG complex, the phenyl ring can adopt a constellation of slightly different orientations relative to the galactose (Fig. 3). In all cases, the phenyl ring is able to make favorable non-polar interactions with the binding surface of the protein, mainly with residue Tyr12.

The BAPG and PEPG ligands were designed to contain a substructure that is isosteric with MNPG, in which the nitro group of MNPG is replaced by a linking amide (Fig. 1*a*). The intent was that the carbonyl O atom of the linking amide would displace the bound water at site #2. This

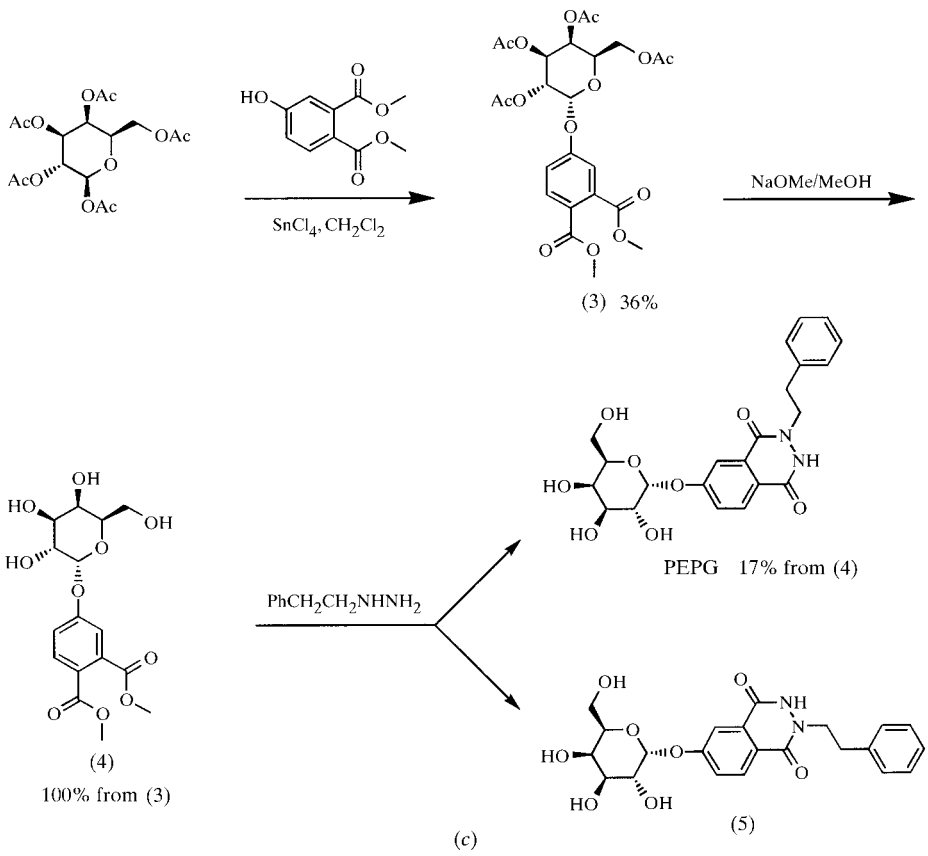

Figure 1 (continued)
(*c*) Synthesis scheme of 2-phenethyl-7-(2,3-dihydrophthalazine-1,4-dione)-α-D-galactoside (PEPG).

displacement did not occur in any of the observed binding modes, however. In the case of BAPG, the failure may result from a preference of the ligand for a *trans* amide rather than a *cis* amide. The *trans* conformation, observed in the present structure, would place ligand atom C1* too close to Gly33 if the benzamido ring were in exactly the same conformation as the ring in MNPG. A second possibility is that there is sufficient difference in the electronic state of the amide carbonyl compared with the MNPG nitro group that substitution into the existing network of hydrogen bonding by displacement of the water is not as favorable. This possibility is bolstered by the fact that this same failure to displace the water at site #2 was found for the ligand *m*-carboxyphenyl-α-D-galactoside (MCPG), which is identical to MNPG except for the substitution of a $-CO_2^-$ group for the $-NO_2$ group in MNPG. Furthermore, the conformation of the benzamido ring in the tertiary binding mode of BAPG is essentially identical to one of the binding modes found for MCPG (Minke *et al.*, 2000). Finally, in both the primary and tertiary binding modes the terminal phenyl group of the ligand is in hydrophobic contact with one of the previously identified patches on the binding surface as hoped. The short linkage from the benzamido group to the terminal phenyl in this compound may be too short to allow both the hydrophobic interaction and the water displacement simultaneously.

The PEPG ligand contains both MNPG and BAPG as isosteric substructures of the rigid phthalhydrazide ring system (Fig. 1). The issue of *cis*/*trans* amide linkage in BAPG has an equivalent in the specific attachment point of the phenethyl group of PEPG. In the compound as synthesized, the attachment is isosteric to a *trans* amide and subject to the same possible steric clash with Gly33 if the binding mode were identical to that of MNPG. As with BAPG, the observed binding mode does not displace the water at site #2, but instead maintains the same protein–ligand hydrogen-bonding network observed to be mediated by this water for galactose derivatives other than MNPG (Merritt, Sixma *et al.*, 1994; Merritt *et al.*, 1997).

In the four well resolved instances of the bound ligand, the additional hydrophobic substituent of PEPG (the phenethyl group) occupies roughly the same portion of the binding site that accommodates an equivalent phenyl group of a minor binding variant of BAPG (Fig. 6*a*) and in the same general area as the glycerol moiety of sialic acid in the GM1-pentasaccharide (Fig. 6*b*). The glycerol moiety of GM1 is not in close contact with the protein surface, however (Merritt *et al.*, 1998), and may be modified or truncated without significantly reducing the binding affinity (Schengrund & Ringler, 1989). In contrast to this, the phenethyl group of PEPG is able to make favorable hydrophobic interactions, in particular with the side chain of residue Lys34

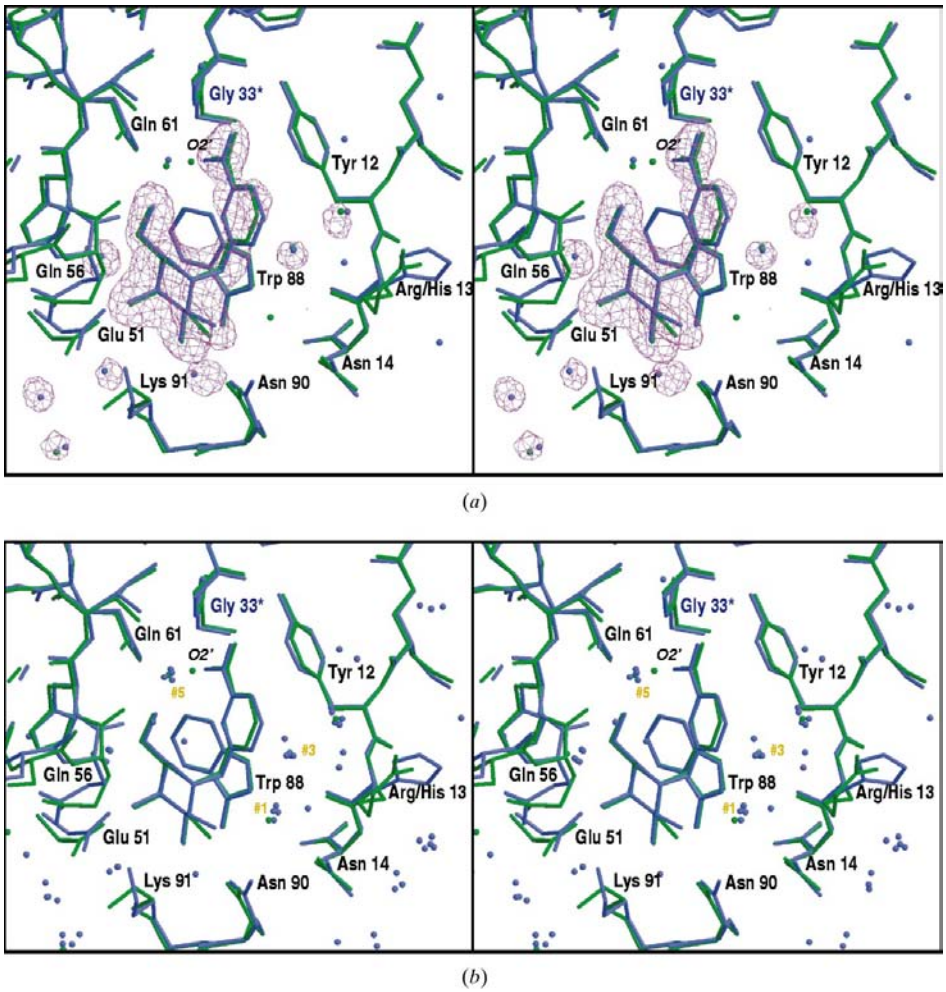

Figure 2
MNPG binding by cholera toxin. Superposition of the binding site of MNPG complexed with the *B* pentamer of two homologous toxins, LT and CT. The LT*B*–MNPG complex (green, PDB code 1lt6; Merritt *et al.*, 1997) was superimposed onto the new structure of the CT*B*–MNPG complex (blue) by least-squares minimization of the coordinate difference for atoms C, N, CA, O, CB of conserved residues within 10 Å of one of the five independent binding sites (site *F* in this figure). The r.m.s. coordinate difference for the 157 superimposed atoms at this site was 0.30 Å. The only sequence difference between the two toxins in the immediate vicinity of the binding site is at residue 13, which is not involved in binding MNPG. (*a*) Electron-density contours at 4σ are shown from a σ_A-weighted omit map ($mF_o - F_c$) of the CT*B*–MNPG complex at 2.0 Å resolution; the five copies of the ligand and all waters within 8 Å were omitted from the calculation of F_c. (*b*) Water molecules identified near all five binding sites have been superimposed back onto site *F*. Consensus water sites #1, #3 and #5 of the receptor-binding site are labeled (numbering as in Merritt, Sixma *et al.*, 1994). The position of water Wat2 is occupied by O2′ of the nitrophenyl group.

and with the peptide unit linking residues Gly33 and Lys34. These residues are from a neighboring subunit which contributes the uppermost portion of the binding surface as seen in Fig. 5. The phenethyl group also closely approaches the hydrophobic surface formed by the side chain of residue Ile58. The ~50-fold increase in binding affinity of PEPG relative to galactose may therefore in part be a consequence of exploitation of hydrophobic interactions in a region of the binding site not optimally complemented by the natural receptor.

This set of structures demonstrates the difficulty of predicting binding constants, or in this case IC_{50} values (Fig. 1*a*), directly from a crystal structure. The average thermal parameters B_{avg} (Table 1) for the ligands in the various refined models do not correlate with the measured IC_{50} values and in the case of the two larger compounds the influence of crystal lattice packing is clear. Nevertheless, it is notable that the compound with the tightest affinity, MNPG, exhibits a single consistent binding mode in the five crystallographically independent sites in the present structure, which are in turn identical to the ten independent sites in the previously reported LT*B*–MNPG complex (Merritt *et al.*, 1997). By contrast PAPG, with poorer affinity, exhibits five distinct conformations among the five crystallographically independent binding sites. BAPG, with an IC_{50} similar to that of PAPG, exhibits three distinct conformations among ten independent sites, although one of these is clearly predominant. It might therefore seem paradoxical that PEPG, with an IC_{50} almost as good as that of MNPG, is found in a well defined conformation in only a minority of the ten independent binding sites. As detailed above, however, this is likely to be an indication that the affinity of this ligand for the binding site is increased by relatively non-specific hydrophobic interactions of the terminal phenethyl group with the upper region of the binding site (Fig. 6).

The galactose derivatives studied have a significantly improved affinity compared with galactose (Fig. 1). The results described in this paper reveal the interactions of additional hydrophobic groups of BAPG and PEPG with a hydrophobic portion of the receptor-binding site which is not exploited by the natural receptor, ganglioside GM1. This favorable interaction provides a basis for the synthesis of novel galactose derivatives targeting this surface of the receptor-binding site. Furthermore, as shown in Fig. 6, different galactose derivatives occupying entirely different regions of the receptor-binding site of LT and CT provide experimental data to guide the design of new ligands combining a variety of favorable interactions with the *B* pentamers which are so far only present in a single galactose derivative. In particular, it will be attractive to use combinatorial chemistry to optimize the length of the linkage to the terminal hydrophobic group of BAPG and PEPG, to investigate terminal groups other than phenyl and to try attachment of substituents at other positions of the phthalhydrazide ring.

4. Experimental procedures

4.1. Crystallization and structure determination of CT*B* in complex with MNPG

Protein buffer used for crystallization initially contained a cholera toxin hybrid hexamer containing a normal *B* pentamer and an engineered *A* subunit (kindly provided by Dr R. K. Holmes) in 10 m*M* Tris pH 7.5, 2 m*M* pepstatin, 2 m*M* PMSF, 5 m*M* DTT, 1 m*M* EDTA and 30 m*M* *m*-nitrophenyl-α-D-galactopyranoside (MNPG) (Sigma N6129). The hybrid toxin hexamer apparently dissociated during crystallization, as only the *B* pentamer was found in the crystal structure. Crystals grew from sitting drops containing 3 µl protein buffer and 3 µl well buffer consisting of 100 m*M* sodium phosphate/citrate pH 4.0 and 19% 1,2-propanediol. Diffraction intensities were measured using Cu $K\alpha$ radiation from a Rigaku RU-200 rotating-anode generator and a Nonius DIP-2030 imaging detector. An initial structural model was constructed by molecular replacement starting from the toxin *B* pentamer as seen in the 1.25 Å structure of the CT*B*–GM1-oligosaccharide complex (Merritt *et al.*, 1998; PDB accession code 3chb). Manual

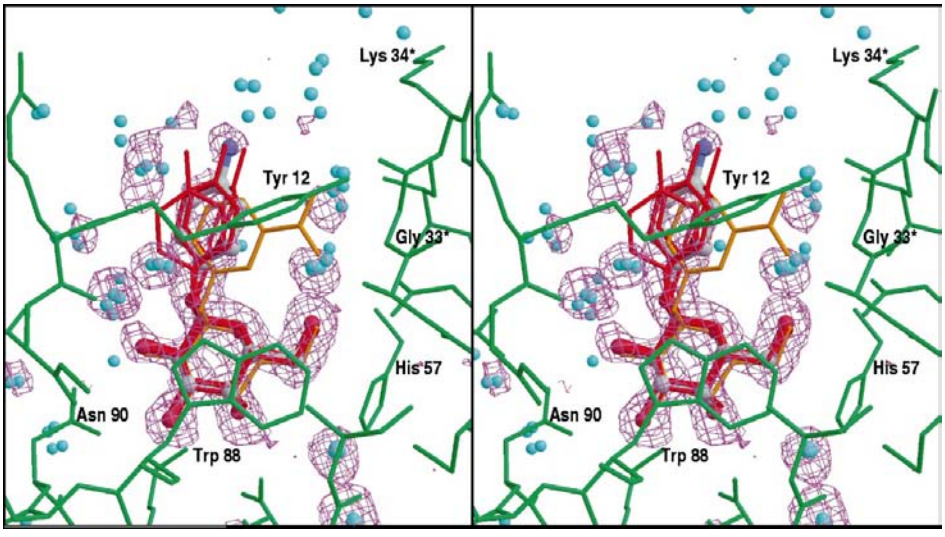

Figure 3
PAPG binding to heat-labile enterotoxin. Stereo pair showing the binding mode of PAPG to the LT *B* pentamer. The protein (green), ball and stick PAPG molecule and 2.5σ electron-density contours are shown for a single binding site (chain *D*) of the LT*B*–PAPG complex. Water molecules (cyan) and the PAPG molecule (red) from the four other copies of the binding site in the present structure are shown superimposed onto this single site to indicate the degree of reproducibility of water placement and the range of conformations seen for the aminophenyl moiety of PAPG. The binding mode of MNPG as seen in the LT*B*–MNPG complex (Merritt *et al.*, 1997) is shown superimposed in gold. Electron density is from an ($mF_o - F_c$) map at 1.6 Å resolution in which all ligand molecules and all water molecules within 8 Å of the binding site were omitted from the calculation of F_c.

rebuilding of side chains, iterative positional and *B*-factor refinement and automated identification of water molecules remote from the receptor-binding site yielded a model with crystallographic residuals R = 0.226, R_{free} = 0.272. At this point, all five copies of the MNPG molecule were fitted into clear electron density of ($mF_o - F_c$) maps. Density at one of the five sites was weaker overall, however, and the MNPG molecule at this site was modeled as having an occupancy of 50%. *B* factors for residues 51–60 of this copy of the binding site were higher than in the remaining four copies, which is consistent with partial occupancy of the ligand at this site. Continued refinement brought the final residuals to R = 0.200, R_{free} = 0.251 (Table 1).

4.2. Crystallization and structure determination of LT*B* in complex with PAPG

Crystals grew from sitting drops by vapor-diffusion equilibration against well buffer containing 100 m*M* sodium citrate/HCl at pH 5.6 and 22%(*w*/*v*) PEG 350 monomethyl ether. Drops consisted of 2 µl protein at 5 mg ml^{-1} of LTB_5 (prepared as described in Minke, Roach *et al.*, 1999) in 20 m*M* HEPES pH 7.5, 2 µl 5 m*M* *p*-aminophenyl-α-D-galactopyranoside (PAPG) (Sigma A8517) and 2 µl well buffer. Diffraction intensities were measured from a single flash-frozen crystal using 1.08 Å radiation from SSRL beamline 7-1 and a MAR image-plate detector. The initial crystallographic model consisted of the previously determined LT *B* pentamer (Merritt *et al.*, 1997; PDB accession code 1lt5) positioned by molecular replacement. Despite possessing similar unit-cell parameters, the present crystals are not isomorphous to the earlier ones. After rigid-body refinement of the constituent LT*B* monomers, the model was rebuilt manually. Iterative positional and *B*-factor refinement, alternating with automated identification of discrete water molecules remote from the sugar-binding sites, yielded crystallographic residuals R = 0.205, R_{free} = 0.2416. At this point, ligand and nearby water molecules were modeled to fit into well defined ($mF_o - F_c$) difference density. After continued refinement, the final model reached crystallographic residuals of R = 0.188, R_{free} = 0.231 with excellent stereochemistry (Table 1).

4.3. Synthesis of BAPG

To a solution of β-D-galactose pentaacetate (14 g, 36 mmol) and 3-hydroxybenzoic acid (5 g, 36 mmol) in 200 ml anhydrous CH_2Cl_2 was added 5 ml (43 mmol) $SnCl_4$. This solution was refluxed for 60 h under N_2 (Fig. 1*b*). The reaction was then allowed to cool to room temperature and quenched by pouring into 200 ml saturated aqueous $NaHCO_3$. The organic

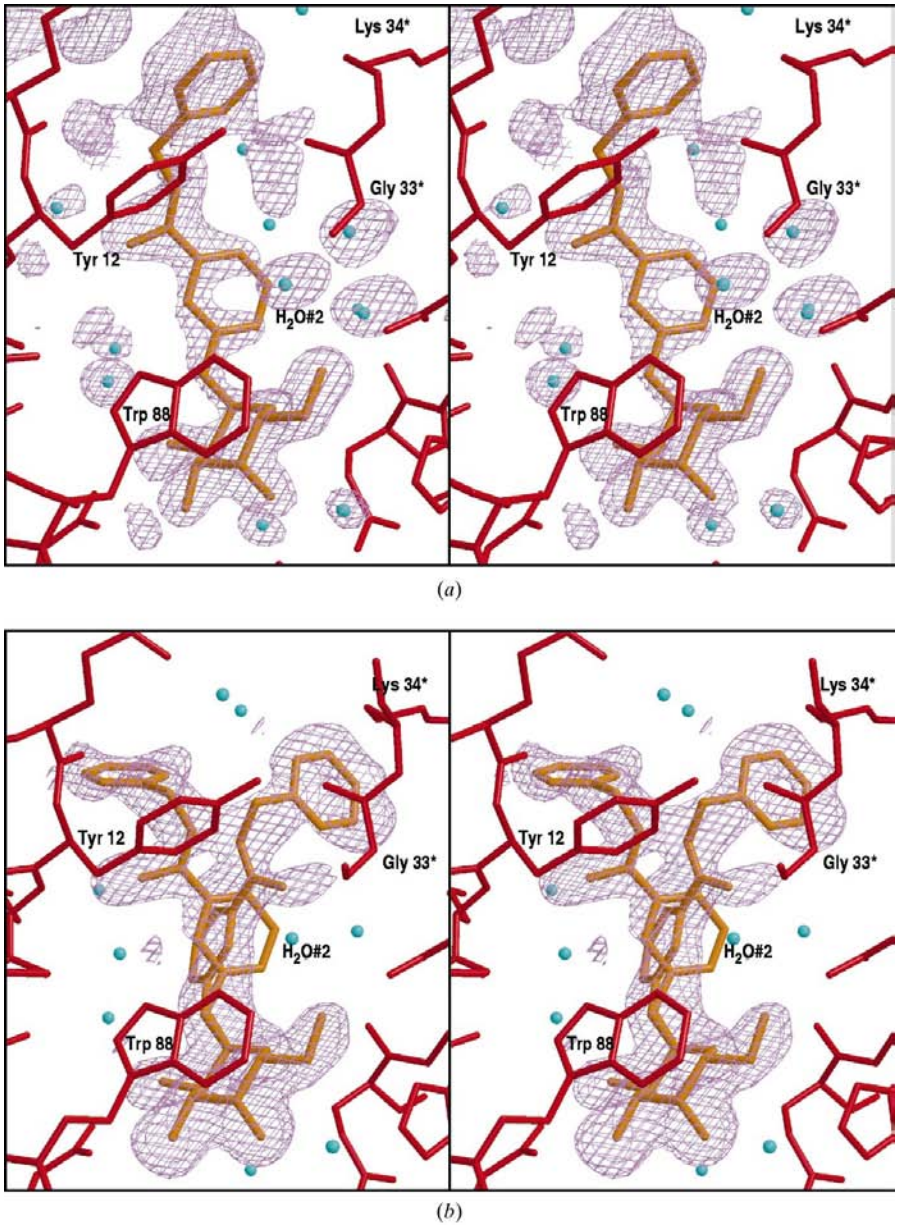

Figure 4
BAPG bound to LT*B*. (*a*) Stereo pair of ($mF_o - F_c$) omit map density at site H showing primary binding mode and conformation of ligand BAPG bound to LT*B*. The terminal phenyl ring of the ligand stacks against the side chain of Tyr12, while atoms N1′ and O1′ of the ligand benzamido ring make water-mediated hydrogen bonds to the protein backbone. (*b*) Stereo pair of ($mF_o - F_c$) omit map density at site *N*. Lattice interactions preclude the primary binding mode for BAPG at this site and instead two alternate conformers are present. The secondary binding mode (left side of figure) differs from the primary conformation only by torsional rotation about the N1′—C1* bond. The tertiary conformer (right side of figure) is similar to the previously observed binding mode of MCPG (Fig. 2). The terminal phenyl ring in this case makes hydrophobic contact with the side chain of Lys34.

layer was then washed extensively with an equal volume of water to remove any residual 3-hydroxybenzoic acid and then concentrated to yield 8.61 g of a pale yellow solid (1). This material, presumably containing a substantial amount of unreacted β-D-galactose pentaacetate, was used without further purification (4% minimum crude yield based on amount of final product obtained).

A small amount of this material (600 mg) was dissolved in ~5 ml of ethyl acetate. Cyanuric chloride (89 mg, 0.48 mmol) was added, followed by 133 µl of *N*-methylmorpholine (NMM). A white precipitate formed immediately upon addition of NMM. The mixture was allowed to stir for 2 h. Benzylamine (139 µl) was then added with continued stirring. 4 h after the addition of benzylamine, the thick mixture was pushed through a syringe filter to remove insoluble by-products. The clear yellow solution was then washed with 2 × 5 ml 10% citric acid followed by 2 × 5 ml saturated NaCl. The organic layer was then dried over $MgSO_4$ and concentrated to give a pale yellow solid. This solid was then dissolved in 5 ml MeOH containing a catalytic amount of sodium metal and allowed to stir for 1 h. The solution was neutralized with a few drops of glacial acetic acid and a small amount was purified by HPLC using a Hewlett–Packard 1100 Series HPLC system (detection at 230 nm, C_{18} column) to give ~40 mg (7%) of the amide compound (2) containing both α and β anomers.

The 40 mg sample was dissolved in 2 ml buffer containing 100 m*M* phosphate and 1 m*M* $MgCl_2$ pH 7. The solution was shaken with ~10 units of β-galactosidase immobilized on acrylic resin overnight. The solution was drained away from the resin and directly subjected to HPLC re-purification yielding 17 mg of the pure α-anomer BAPG which was used for co-crystallization with LT*B* and inhibition assays. ^{1}H NMR of BAPG showed no discernible peak corresponding to the β anomer. ^{1}H NMR (methanol-d_4): δ 7.62–7.28 (m, 9H), 5.57 (s, anomeric 1H), 4.56 (s, 2H), 3.96–3.89 (m, sugar ring, 4H), 3.68 (d, sugar CH_2, 2H). Electrospray-MS: 390.3 $(M + H)^+$, 789.5 (H^+-bridged dimer).

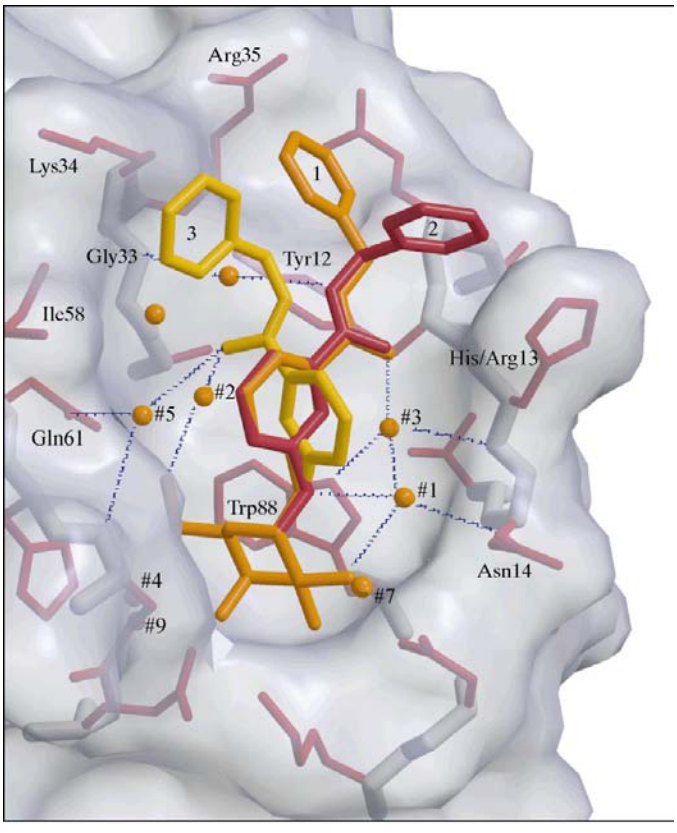

(*c*)

Figure 4 (continued)
(*c*) The three binding modes for compound BAPG observed in the complex with LT*B*. The primary mode is seen in seven of ten crystallographically independent sites. Mode 2 is stabilized by lattice interactions in two sites, but is also present as a secondary binding mode at other sites. The third binding mode is observed in only one site.

4.4. Crystallization and structure determination of LT*B* in complex with BAPG

Crystals grew from sitting drops consisting of 2 µl protein at 2.0 mg ml^{-1} in 100 m*M* Tris–HCl at pH 7.5, 2 µl of a 4 m*M* BAPG in the same buffer and 2 µl well buffer containing 50 m*M* NaCl, 100 m*M* Tris–HCl pH 7.5 and 30%(*w*/*v*) PEG 5000. Diffraction data were measured from a flash-frozen crystal at 110 K using Cu $K\alpha$ radiation from a Rigaku RU-200 rotating-anode generator and a Nonius DIP-2030 imaging-plate detector. The initial molecular-replacement solution was refined to an *R* factor of 0.216 (R_{free} = 0.271), at which point the ligand was fitted into clear density at all sites. Further refinement and manual refitting yielded the final crystallographic model described in Table 1.

4.5. Synthesis of PEPG

To a solution of β-D-galactose pentaacetate (1.45 g, 3.7 mmol) and dimethyl 4-hydroxyphthalate (0.50 g, 2.4 mmol) in 10 ml CH_2Cl_2 was added 0.4 ml $SnCl_4$. This solution was refluxed overnight (Fig. 1*c*). After removal of solvent, the crude mixture was subjected to chromatographic purification on silica gel with 2:1 ether:hexane as eluent. Pure (3) was isolated. Yield: 0.46 g, 36%. ^{1}H NMR ($CDCl_3$): δ 7.80 (d, 1H), 7.30 (d, 1H), 7.19 (dd, 1H), 5.85 (d, 1H), 5.56–5.51 (m, 2H), 5.30 (dd, 1H), 4.26 (dt, 1H), 4.11–4.04 (m, 2H), 3.91 (s, 3H), 3.88 (s, 3H), 2.17 (s, 3H), 2.07 (s, 3H), 2.03 (s, 3H), 1.94 (s, 3H). Electrospray-MS: 541 $(M + H)^+$, 563 $(M + Na)^+$.

Part of the above pure product (0.153 g, 0.283 mmol) was first dissolved in anhydrous MeOH and a catalytic amount of sodium methoxide was then added. The solution was stirred at room temperature for 30 min. Neutralization with cation-exchange resin (H^+ form) and removal of solvent gave pure deprotected sugar compound (4) in quantitative yield. ^{1}H NMR (acetone-d_6): δ 7.78 (d, 1H), 7.35 (d + dd, 2H), 5.65 (d, 1H), 4.04–3.96 (m, 5H), 3.86–3.84 (m, 2H), 3.84 (s, 3H), 3.83 (s, 3H), 3.72–3.67 (m, 3H). Electrospray-MS: 373 $(M + H)^+$. This compound was added to 20 ml water containing 8.55 mmol phenethyl hydrazine (generated by dissolving 2.0 g of the hydrazine sulfate and neutralized with anionic exchange resin in the OH^- form). The solution was heated to reflux

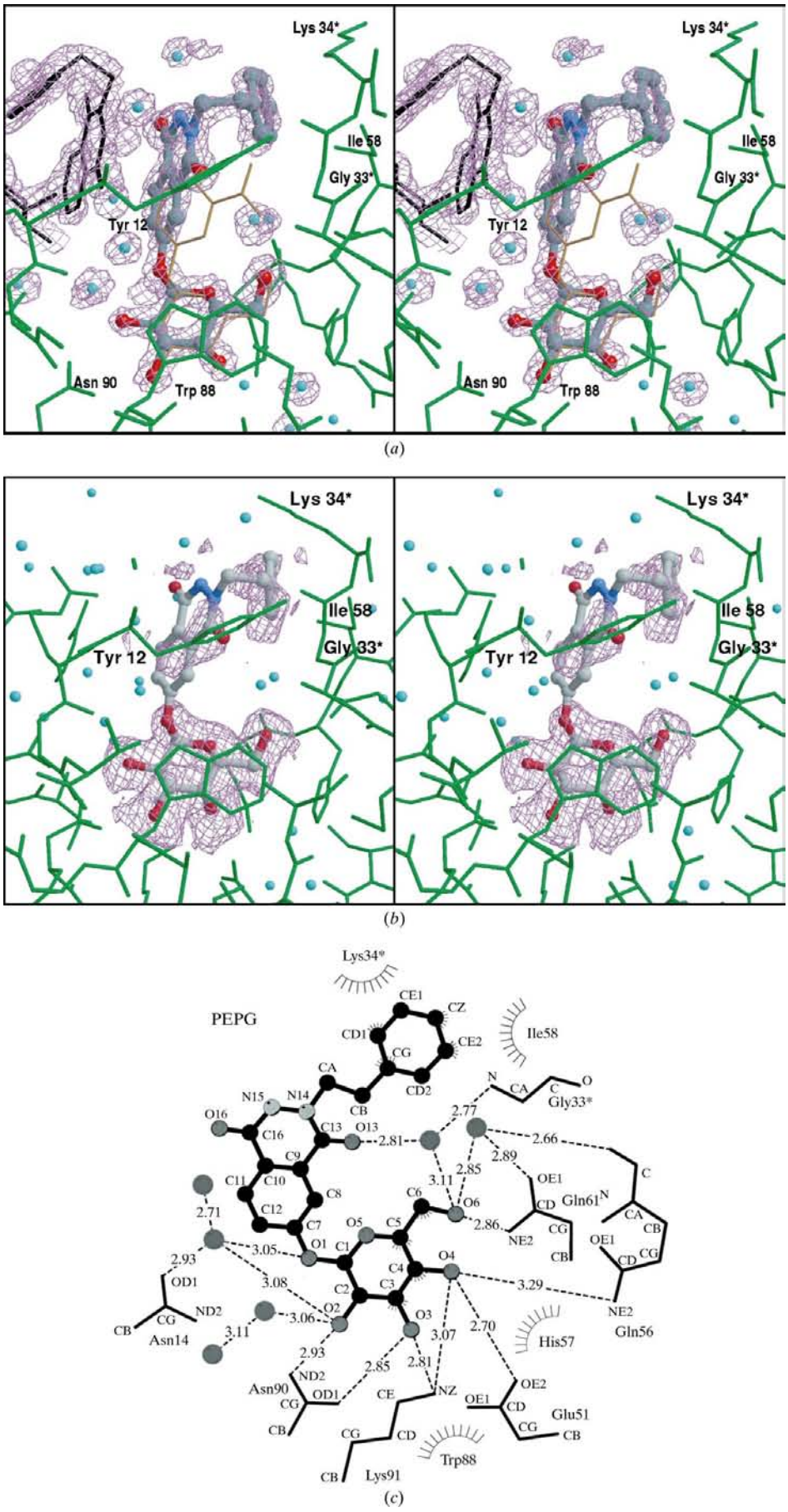

under nitrogen for 4 d. At this time, all sugar starting material was consumed. The excess hydrazine was removed by treatment with cation-exchange resin in the H^+ form. The resulting aqueous solution was neutralized with NaOH to pH 5–6. Removal of solvent gave crude products. TLC (silica gel, 30% $MeOH/CH_2Cl_2$) showed two products in equal amounts. ^1H NMR of this product mixture also showed two sets of phthalyl proton signals in roughly equal amounts. [MeOH-d_4: δ, set one, 8.01 (d, 1H), 7.97 (d, 1H), 7.65 (dd, 1H); set two, 8.21 (d, 1H), 7.73 (d, 1H), 7.61 (dd, 1H); overlapping sets of other proton signals, 7.25–7.16 (m, 2 × 5H), 5.74 (s, 2 × 1H), 4.29–4.24 (m, 2 × 2H), 4.01–3.97 (m, 2 × 3H), 3.86–3.84 (M, 2 1H), 3.70–3.66 (m, 2 × 2H), 3.11–3.08 (m, 2 × 2H)]. Electrospray-MS: 445 $(M + H)^+$, 467 $(M + Na)^+$. This evidence suggested that two isomeric forms of the product were obtained. The first isomer is PEPG (Fig. 1), with the phenethyl moiety attached to N14. The second isomer could be the product with the phenethyl substitution on the other N atom [compound (5)]. When the product mixture was dissolved in a small amount of MeOH, a precipitate was

Figure 5
PEPG bound to LT*B*. (*a*) Stereo pair showing the binding mode of PEPG (Fig. 1) to the LT*B* pentamer. The site shown in this figure is one of four in which a lattice interaction allows stacking of the conjugated ring system with a non-crystallographic symmetry-related molecule (black lines at upper left). The binding mode of MNPG as seen in the LT*B*–MNPG complex (Merritt *et al.*, 1997; PDB code 1lt6) is shown in gold. Electron-density contours at 4.5σ are shown for a σ_A-weighted ($mFo - F_c$) map at 1.8 Å resolution in which all copies of the ligand and all waters within 6 Å were omitted from F_c. (*b*) Electron density of a subunit in which PEPG is not involved in crystal contacts. Stereo pairing showing ($mF_o - F_c$) difference electron density at the binding site of subunit M of the LT*B*–PEPG complex. The ligand-binding mode shown in (*a*) is superimposed on 1.5σ density contours. (*c*) Protein–ligand interactions between LT*B* and compound PEPG.

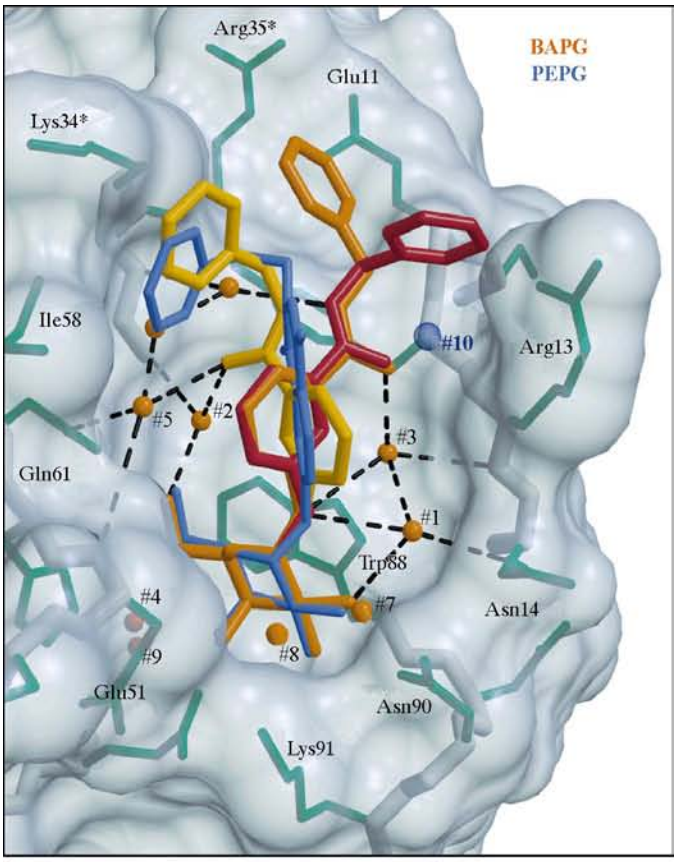

(*a*)

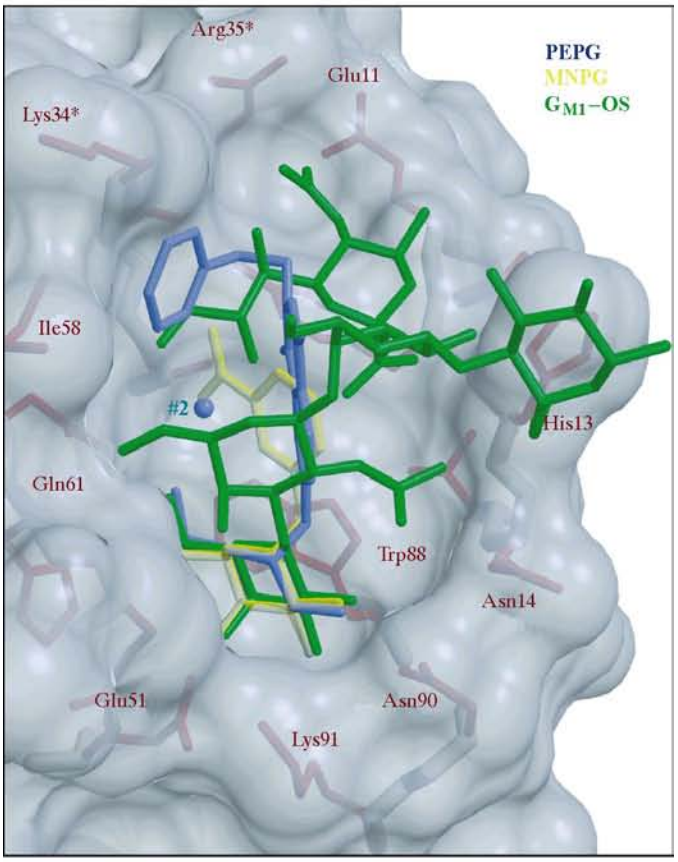

(*b*)

obtained. TLC analysis showed that it contained the faster moving product PEPG with a minor contamination of the slower moving product (5). This sample of PEPG was then used for co-crystallization experiments with LT*B*. The isolated yield of the isomer (5) was too low for further studies. Yield of PEPG: 0.021 g, 17%. ^{1}H NMR (MeOH-d_4) showed the set of phthalyl proton signals at δ 8.01, 7.97 and 7.65.

4.6. Crystallization and structure determination of LT*B* in complex with PEPG

Crystals grew from sitting drops consisting of 1 µl protein containing 2.5 mg ml^{-1} of LT-B_5 (obtained as described in Minke, Roach *et al.*, 1999) in 10 m*M* HEPES pH 7.5, 1 µl of a saturated solution of PEPG in 50% acetone and 50% 10 m*M* HEPES pH 7.5 and 1 µl well buffer containing 100 m*M* cacodylate pH 6.5, 200 m*M* $MgCl_2$ and 35% 2-propanol. Diffraction intensities were measured from a flash-frozen crystal at 110 K using Cu $K\alpha$ radiation from a Rigaku RU-200 rotating-anode generator and a Nonius DIP-2030 imaging detector. The space group of the crystals is somewhat problematic; the unit cell is nearly identical to previous LT*B* structures determined in space group *C*2 (Merritt *et al.*, unpublished work), but in the present case the *C*2 symmetry is imperfect and the $h + k$ = odd diffraction net is weak but not absent. We chose to treat the cell contents as two independent toxin pentamers per asymmetric unit in space group $P2_1$ (Table 1). Difference density ($mF_o - F_c$) maps were examined after initial molecular replacement and rigid-body refinement of the ten protein subunits, manual rebuilding of some side chains, iterative refinement and placement of discrete water molecules remote from the sugar-binding sites. Excellent electron density existed at all ten binding sites for the α-D-galactopyranose moiety of the bound PEPG. Density corresponding to the remainder of the molecule was clear in four of the ten sites for which lattice packing allows a stacking interaction between non-crystallographic symmetry-related copies of the conjugated ring system (Fig. 4*a*). Continued refinement of a model including four complete and six incomplete ligand molecules yielded final crystallographic residuals of R = 0.182, $R_{\rm free}$ = 0.267 (Table 1).

Figure 6
(*a*) Superposition of the binding modes observed for compounds BAPG (yellow, orange, red) and PEPG (blue) onto the molecular surface of the receptor-binding site of LT*B*, showing the range of conformations adopted in positioning the terminal phenyl ring of the ligand against the extended hydrophobic surface of the binding site in the upper portion of the figure. The locations of highly conserved sites for bound water molecules are shown with numbering as in Merritt, Sarfaty *et al.* (1994). (*b*) Superposition of the binding modes for compounds MNPG (yellow) and the full pentasaccharide from the natural receptor ganglioside GM1 (green) onto the molecular surface of the receptor-binding site of CT*B* as seen in the 1.25 Å structure of the CT*B* + GM1-oligosaccharide complex (Merritt *et al.*, 1998). The water at site #2, displaced by MNPG but not by PEPG or by the receptor, is also shown. The receptor-binding sites of LT*B* and CT*B* differ only at residue 13, visible at the right of both (*a*) and (*b*), which is an arginine in LT*B* from porcine strains of *E. coli* and histidine in cholera toxin and in LT*B* from human strains of *E. coli*.

4.7. Crystallographic computation

In all cases, intensity data were merged and scaled using programs *DENZO*, *SCALEPACK* and *TRUNCATE* (Collaborative Computational Project, Number 4, 1994; Otwinowski & Minor, 1997). The program *AMoRe* (Navaza, 1994) was used for molecular replacement and *Xfit* (McRee, 1993) for model building and map interpretation. The LT*B*–BAPG complex was refined using *REFMAC* version 4.0 (Collaborative Computational Project, Number 4, 1994); the other three structures were refined using *X-PLOR* 3.851 (Brünger, 1996). The structural models included a Babinet bulk-solvent model and an overall anisotropic *B* correction, both of which were applied as a correction to F_c during refinement and map fitting. Figures were prepared using programs *MSMS* (Sanner *et al.*, 1996), *Raster3D* (Merritt & Bacon, 1997) and *Ligplot* (Wallace *et al.*, 1995).

This work was supported by the NIH (grant AI44954 to EF; grant AI34501 to WGJH) and by the Murdock Charitable Trust. The engineered cholera toxin used in crystallization was generously provided by Randall K. Holmes and Jerrod L. Erbe, University of Colorado, Denver, CO. We thank Stephen Sarfaty and Misol Ahn for crystal growth and Wendy Minke and Christophe Verlinde for discussions and suggestions. Several crystallographic data sets were collected at the Stanford Synchrotron Radiation Laboratory (SSRL), which is funded by the Department of Energy, Office of Basic Energy Sciences. The Biotechnology Program at SSRL is supported by the National Institutes of Health, National Center for Research Resources, Biomedical Technology Program and the Department of Energy, Office of Biological and Environmental Research.

References

Akker, F. van den, Steensma, E. & Hol, W. G. J. (1996). *Protein Sci.* **5**, 1184–1188.
Brünger, A. T. (1996). *Methods Mol. Biol.* **56**, 245–266.
Collaborative Computational Project, Number 4 (1994). *Acta Cryst.* D**50**, 760–763.
Eidels, L., Proia, R. L. & Hart, D. A. (1983). *Microbiol. Rev.* **47**, 596–620.
Holmgren, J. & Svennerholm, A. M. (1992). *Gastroenterol. Clin. North Am.* **21**, 283–302.
McRee, D. (1993). *Practical Protein Crystallography.* San Diego, Academic Press.
Merritt, E. A. & Bacon, D. J. (1997). *Methods Enzymol.* **277**, 505–524.
Merritt, E. A., Kuhn, P., Sarfaty, S., Erbe, J. L., Holmes, R. K. & Hol, W. G. J. (1998). *J. Mol. Biol.* **282**, 1043–1059.
Merritt, E. A., Sarfaty, S., van den Akker, F., L'hoir, C., Martial, J. A. & Hol, W. G. J. (1994). *Protein Sci.* **3**, 166–175.
Merritt, E. A., Sarfaty, S., Feil, I. K. & Hol, W. G. J. (1997). *Structure*, **5**, 1485–1499.
Merritt, E. A., Sixma, T. K., Kalk, K. H., van Zanten, B. A. M. & Hol, W. G. J. (1994). *Mol. Microbiol.* **13**, 745–753.
Minke, W. E., Diller, D. J., Hol, W. G. J. & Verlinde, C. L. M. J. (1999). *J. Med. Chem.* **42**, 1778–1788.
Minke, W. E., Hong, F., Verlinde, C. L. M. J., Hol, W. G. J. & Fan, E. (1999). *J. Biol. Chem.* **274**, 33469–33473.
Minke, W. E., Pickens, J., Merritt, E. A., Fan, E., Verlinde, C. L. M. J. & Hol, W. G. J. (2000). *Acta Cryst.* D**56**, 795–804.
Minke, W. E., Roach, C., Hol, W. G. J. & Verlinde, C. L. M. J. (1999). *Biochemistry*, **38**, 5684–5692.
Navaza, J. (1994). *Acta Cryst.* A**50**, 157–163.
Otwinowski, Z. & Minor, W. (1997). *Methods Enzymol.* **276**, 307–326.
Sanner, M. F., Olson, A. J. & Spehner, J. C. (1996). *Biopolymers*, **38**, 305–320.
Schengrund, C.-L. & Ringler, N. J. (1989). *J. Biol. Chem.* **264**, 13233–13237.
Simeant, S. (1992). *World Heath Stat. Q.* **45**, 208–219.
Sixma, T. K., Kalk, K. H., van Zanten, B. A. M., Dauter, Z., Kingma, J., Witholt, B. & Hol, W. G. J. (1993). *J. Mol. Biol.* **230**, 890–918.
Sixma, T. K., Pronk, S. E., Kalk, K. H., van Zanten, B. A. M., Berghuis, A. M. & Hol, W. G. J. (1992). *Nature (London)*, **355**, 561–564.
Sixma, T. K., Pronk, S. E., Kalk, K. H., Wartna, E. S., van Zanten, B. A. M., Witholt, B. & Hol, W. G. J. (1991). *Nature (London)*, **351**, 371–377.
Wallace, A. C., Laskowski, R. A. & Thornton, J. M. (1995). *Protein Eng.* **8**, 127–134.
Wanke, C. A., Lima, A. A. & Guerrant, R. L. (1987). *Baillieres Clin. Gastroenterol.* **1**, 335–359.